J. Fluid Mech. (2005), *vol.* 535, *pp.* 325–345.
doi:10.1017/S0022112005004866 Printed in the United Kingdom

Hydrodynamic model for a vibrofluidized granular bed

By T. W. MARTIN, J. M. HUNTLEY AND R. D. WILDMAN

Wolfson School of Mechanical and Manufacturing Engineering, Loughborough University, Loughborough, Leicestershire, LE11 3TU, UK

(Received 30 January 2003 and in revised form 14 February 2005)

Equations relating the energy flux, energy dissipation rate, and pressure within a three-dimensional vibrofluidized bed are derived and solved numerically, using only observable system properties, such as particle number, size, mass and coefficient of restitution, to give the granular temperature and packing fraction distributions within the bed. These are compared with results obtained from positron emission particle tracking experiments and the two are found to be in good agreement, without using fitting parameters, except at high altitudes when using a modified heat law including a packing fraction gradient term. Criteria for the onset of the Knudsen regime are proposed and the resulting temperature profiles are found to agree more closely with the experimental distributions. The model is then used to predict the scaling relationship between the height of the centre of mass and mean weighted bed temperature with the number of particles in the system and the excitation level.

1. Introduction

Many industries use solid materials in granular form, and these granules have to be stored, transported, and processed. However, often relatively little is known about their behaviour during these stages; most processes that are used work satisfactorily, but the reasons why are not always clear. Thus whilst there is a wealth of information for specific particles in various systems, this is often only applicable to the system investigated, and a more general approach is required. Of particular use for dilute mobile granular flows is the analogy that the particles behave like the atoms or molecules in a gas, albeit with the important distinction that the collisions in this macroscopic gas are dissipative, and so require an energy input to sustain the behaviour.

The system we consider here has energy supplied by a horizontal plate vibrating in the vertical direction, which supplies energy to particles above it by impact; the energetic particles then form the familiar gaslike state. Such a system has been extensively investigated both by models and experiments covering one (Luding *et al.* 1994*a*), two (Kumaran 1998*a*), and three (Bizon *et al.* 1999) dimensions and employing such methods as high-speed photography (Warr, Huntley & Jacques 1995; Horluck & Dimon 2001), magnetic resonance imaging (Yang *et al.* 2002) and positron emission particle tracking (PEPT) (Wildman *et al.* 2000), with a fair degree of agreement between the two. The most accurate models use molecular dynamics or discrete element modelling (DEM) to model the motion of each grain in the bed, but these approaches are computationally intensive, especially when the deformation of the particles is taken into account in DEM. Another approach is analytical modelling (Brey, Moreno & Dufty 1996), where the hydrodynamic equations initially derived for

classical gases are adapted and applied to this granular gas. The main advantage of such an approach is that it is much quicker to solve these coupled differential equations than it is to perform particle level simulations, although the information gained may be more limited, and the whole is dependent upon the molecular gas analogy outlined above.

Validation of these mathematical models by comparison with the results of numerical simulations and/or experiments is clearly an important step in establishing the range of operating parameters over which they apply. Lan & Rosato (1995) and Helal, Biben & Hansen (1997), for example, compared the predictions of one-dimensional hydrodynamic models to discrete element and molecular dynamics simulations with reasonable agreement, but in the latter case, constants were adjusted to fit the model to the observed results. What we attempt to do here is to use the most appropriate form of both the hydrodynamic equations and the boundary conditions for the system, to predict the packing fraction and granular temperature distributions within the system, without using any fitting parameters. Without such parameters, the selection of the correct equations, from those available in print (e.g. Chapman & Cowling 1970; Jenkins & Savage 1983), to describe the system is vital; these equations are presented in the next section. We then compare these results to distributions of packing fraction and granular temperature measured experimentally within a three-dimensional bed using PEPT.

2. The hydrodynamic model

The system that we are attempting to model here is a vibrofluidized bed, consisting of a container with particles inside, which rests upon a vibrating platform. Collisions between the particles and the moving base supply energy to the system, while particle and wall collisions remove energy from the system. In this analysis, a hollow cylinder, of radius R, and of a height sufficient to contain all important events (typically 50 particle diameters) is used. Into this cylinder are placed N particles each with a diameter d and a mass m. The system is then vibrated sinusoidally in the vertical direction at a given frequency ω and a displacement amplitude A_0.

Within this vibrating system, two conditions must be met to give a stable solution. First, the weight of a section of the expanded bed must be supported by the particles below it and it must, in turn, support the weight of the particles above, in much the same way as a classical gas. Unlike such a gas though, the collisions within this system are inelastic, so with each one, kinetic energy is lost from the system to heat and plastic deformation. Two types of collision can occur: particle–particle and particle–wall. So secondly, to balance these losses, particles colliding with the vibrating base will gain energy. If the base does not provide sufficient power, a fluidized bed is not formed, although other behaviour such as shock waves, quasi-static convection and particle rearrangement, can be observed (Clément *et al.* 1996).

The distribution of particles is conveniently represented by the packing fraction field, $\eta(x, y, z)$, which indicates the fraction of the space taken up by particles in a volume element located at any point (x, y, z). The mean fluctuation kinetic energy of the particles is commonly known as the granular temperature, $E_0(x, y, z)$, by analogy with the thermodynamic property of a classical gas. With experimental PEPT data, this can be obtained from the time variation of the mean squared particle displacement (Wildman & Huntley 2000).

The approach taken by Helal *et al.* (1997) involved approximating two-dimensional fields by one-dimensional profiles in the vertical (z) direction. The force balance condition combined with an equation of state resulted in a first-order ordinary differential equation (ODE) for $\eta(z)$. The combination of an energy balance condition together with a heat flux equation gave a second-order ODE for $E_0(z)$. Solution of these two coupled ODEs required three boundary conditions, which were obtained by fitting to the results of a molecular dynamics simulation. We follow a similar approach, but use more appropriate expressions for the equation of state, the energy balance expression (which includes wall dissipation), and the heat flux equation, as well as for the boundary conditions at the base, and furthermore involve no adjustable parameters.

The force balance equation is

$$\frac{\mathrm{d}P}{\mathrm{d}z} = -\rho g = -\frac{6}{\pi d^3}\eta m g, \tag{2.1}$$

where P is the pressure within the bed, ρ is the mass density, and g is the acceleration due to gravity.

The relationship between pressure and temperature for an ideal gas is given by the simple kinematic equation of state:

$$P = \frac{6k_B}{\pi d^3}\eta T, \tag{2.2}$$

where k_B is the Boltzmann constant and T is the thermodynamic temperature. However, this does not take into account the fraction of the volume occupied by the particles. An alternative equation of state for a system of macroscopic particles, which is more accurate at higher packing fractions, has been proposed by Carnahan & Starling (1969)

$$P = \frac{6k_B}{\pi d^3}\frac{\eta(1+\eta+\eta^2-\eta^3)}{(1-\eta)^3}T. \tag{2.3}$$

Here it is assumed that the distribution of individual particle velocities follows a Maxwell–Boltmann distribution, so that the granular temperature can be defined as $E_0 = k_B T = m\langle v^2\rangle$, with $\langle v^2\rangle$ being the mean squared fluctuation velocity in any given direction. The two equations of state are of a similar form and the second, (2.3), more realistic one will be used here.

Differentiating (2.3) with respect to height, and equating to the right-hand side of (2.1) gives the variation of the packing fraction with height, as a function of the packing fraction, temperature and temperature gradient. For convenience, we convert the variables z and T into the dimensionless quantities z^* and T^*, using the relationships $z^* = z/d$ and $T^* = k_B T/mgd$. This gives

$$\frac{\mathrm{d}\eta}{\mathrm{d}z^*} = -\frac{\eta}{T^*}\frac{(1-\eta)^4}{(1+4\eta+4\eta^2-4\eta^3+\eta^4)}\left(1+\frac{(1+\eta+\eta^2-\eta^3)}{(1-\eta)^3}\frac{\mathrm{d}T^*}{\mathrm{d}z^*}\right). \tag{2.4}$$

Unlike the case of an isothermal ideal gas, the presence of energy dissipation means that the $\mathrm{d}T^*/\mathrm{d}z^*$ term cannot be assumed to be zero. For completeness, we also give the second derivative of η, which will be required later:

$$\frac{\mathrm{d}^2\eta}{\mathrm{d}z^{*2}} = f(\eta, T^*) - \frac{\eta}{T^*}\frac{(1-\eta)(1+\eta+\eta^2-\eta^3)}{(1+4\eta+4\eta^2-4\eta^3+\eta^4)}\frac{\mathrm{d}^2T^*}{\mathrm{d}z^{*2}}, \tag{2.5}$$

where

$$
\begin{aligned}
f(\eta, T^*) = &-\frac{1}{T^*}\frac{(1-\eta)^4}{(1+4\eta+4\eta^2-4\eta^3+\eta^4)}\frac{\mathrm{d}\eta}{\mathrm{d}z^*} + \frac{4\eta}{T^*}\frac{(1-\eta)^3}{(1+4\eta+4\eta^2-4\eta^3+\eta^4)}\frac{\mathrm{d}\eta}{\mathrm{d}z^*} \\
&+\frac{\eta}{T^*}\frac{4(1+2\eta-3\eta^2+\eta^3)(1-\eta)^4}{(1+4\eta+4\eta^2-4\eta^3+\eta^4)^2}\frac{\mathrm{d}\eta}{\mathrm{d}z^*} + \frac{\eta}{T^{*2}}\frac{(1-\eta)^4}{(1+4\eta+4\eta^2-4\eta^3+\eta^4)}\frac{\mathrm{d}T^*}{\mathrm{d}z^*} \\
&-\frac{1}{T^*}\frac{(1-\eta)(1+\eta+\eta^2-\eta^3)}{(1+4\eta+4\eta^2-4\eta^3+\eta^4)}\frac{\mathrm{d}T^*}{\mathrm{d}z^*}\frac{\mathrm{d}\eta}{\mathrm{d}z^*} \\
&+\frac{\eta}{T^*}\frac{(1+\eta+\eta^2-\eta^3)}{(1+4\eta+4\eta^2-4\eta^3+\eta^4)}\frac{\mathrm{d}T^*}{\mathrm{d}z^*}\frac{\mathrm{d}\eta}{\mathrm{d}z^*} \\
&-\frac{\eta}{T^*}\frac{(1-\eta)(1+2\eta-3\eta^2)}{(1+4\eta+4\eta^2-4\eta^3+\eta^4)}\frac{\mathrm{d}T^*}{\mathrm{d}z^*}\frac{\mathrm{d}\eta}{\mathrm{d}z^*} \\
&+\frac{\eta}{T^*}\frac{4(1+2\eta-3\eta^2+\eta^3)(1-\eta)(1+\eta+\eta^2-\eta^3)}{(1+4\eta+4\eta^2-4\eta^3+\eta^4)^2}\frac{\mathrm{d}T^*}{\mathrm{d}z^*}\frac{\mathrm{d}\eta}{\mathrm{d}z^*} \\
&+\frac{\eta}{T^{*2}}\frac{(1-\eta)(1+\eta+\eta^2-\eta^3)}{(1+4\eta+4\eta^2-4\eta^3+\eta^4)}\left(\frac{\mathrm{d}T^*}{\mathrm{d}z^*}\right)^2. \qquad (2.6)
\end{aligned}
$$

The second condition for the system to exist in a steady state is the energy balance requirement: the energy entering a section of the bed in a unit time must equal the amount leaving the section plus the amount lost in that section in a unit time owing to collisions. In this system, the energy entering a horizontal slice of the cylinder is given by the upward flux of energy through the bed. We compare here three different equations that have been proposed relating this flux to the temperature and packing fraction gradients.

In the simplest model, the energy flux, $\boldsymbol{J}$, is dependent only upon the temperature gradient, as stated by Fourier's law of heat conduction, and a typical expression for this when applied to a granular system is given by Kay & Nedderman (1985)

$$\boldsymbol{J} = -\kappa\nabla T, \qquad (2.7)$$

where

$$\kappa = \frac{6\eta k_B^2 T}{\pi d^3 m\zeta}, \qquad (2.8)$$

and where ζ is the single particle collision rate.

However, more recent work has also incorporated a second term, proportional to the packing fraction gradient, into the energy flux expression, which takes into account the energy transfer rate given by the variation in packing fraction concentration owing to the presence of inelastic particles. This revised expression has been developed by Brey *et al.* (1996), and more recently adapted to the system of interest here by Brey *et al.* (1998), and has the form

$$\boldsymbol{J} = -\kappa\nabla T - \mu\nabla\eta, \qquad (2.9)$$

where

$$\kappa = \kappa^*\kappa_0, \qquad (2.10)$$

$$\mu = \mu^*\frac{T}{\eta}\kappa_0, \qquad (2.11)$$

where the coefficients $\kappa*$ and $\mu*$ are dimensionless functions of the inter-particle coefficient of restitution, e (tending to 1 and 0, respectively, as e tends to 1), which

alter the basic thermal conductivity, κ_0, given by

$$\kappa_0 = \frac{75k_B}{64d^2}\left(\frac{k_BT}{\pi m}\right)^{1/2}. \tag{2.12}$$

$\kappa*$ and $\mu*$ are given by

$$\kappa^* = \tfrac{2}{3}(1 + c(e))(\nu(e) - 2\zeta(e))^{-1}, \tag{2.13}$$

$$\mu^* = 2\zeta(e)\left(\kappa^* + \frac{c(e)}{3\zeta(e)}\right)(2\nu(e) - 3\zeta(e))^{-1}, \tag{2.14}$$

and

$$c(e) = \frac{32(1-e)(1-2e^2)}{(81 - 17e + 30e^2(1-e))}, \tag{2.15}$$

$$\zeta(e) = \tfrac{5}{12}(1-e^2)\left(1 + \frac{3c(e)}{32}\right), \tag{2.16}$$

$$\nu(e) = \tfrac{1}{3}(1+e)\left(1 + \frac{33(1-e)}{16} + \frac{(19-3e)c(e)}{1024}\right). \tag{2.17}$$

In the perfectly elastic limit, (2.10)–(2.17) reduce to (2.8) except for a scaling factor of 75/16.

The third expression for energy flux considered here is given by Jenkins (1999). This retains only the temperature gradient term, but unlike the Brey expression contains extra terms that account for excluded volume effects at high packing fractions:

$$\kappa = \frac{45}{8}\frac{\eta}{\sqrt{\pi}d^2}\left(\frac{k_B^3T}{m}\right)^{1/2}\left[\frac{5}{24}\frac{1}{G} + 1 + \frac{6}{5}\left(1 + \frac{32}{9\pi}\right)G\right], \tag{2.18}$$

where

$$G = \eta g_0(\eta) = \frac{\eta(2-\eta)}{2(1-\eta)^3}, \tag{2.19}$$

and $g_0(\eta)$ is the pair distribution function at contact, which increases the collision rate due to excluded volume effects. In this work, $g_0(\eta)$ is taken to be that given by Jenkins & Savage (1983), namely

$$g_0(\eta) = \frac{2-\eta}{2(1-\eta)^3}. \tag{2.20}$$

Again, in the dilute limit, (2.18) and (2.19) reduce to (2.8) except for a scaling factor of 75/16.

Equations (2.9)–(2.19) can be used to specify the transfer of energy into and out of a volume element, and consequently the change in flux over the region. Before doing this, however, we must specify the energy dissipation due to collisions with the wall and other particles. Jenkins & Savage (1983) calculate the grain–grain dissipation rate, γ_{gg}, by multiplying the mean collision frequency by the mean energy loss per collision, which can be written as

$$\gamma_{gg} = \frac{72\eta^2 g_0(\eta)(1-e^2)}{\pi^{3/2}d^4}\left(\frac{k_B^3T^3}{m}\right)^{1/2}, \tag{2.21}$$

and in the manner of Wildman, Huntley & Parker (2001) another expression for the particle–wall dissipation rate per unit area and time, γ_{gw}, is obtained:

$$\gamma_{gw} = \frac{3\eta\chi(\eta)\left(1-e_w^2\right)}{(2\pi)^{3/2}d^3}\left(\frac{k_B^3T^3}{m}\right)^{1/2}, \tag{2.22}$$

where e_w is the particle–wall coefficient of restitution, and $\chi(\eta)$ is the enhancement factor for particles hitting the wall, owing to the presence of other particles, as derived by Pasquarell & Ackermann (1989), and given by

$$\chi(\eta) = \frac{(1-2\eta)}{(1-4\eta)}. \tag{2.23}$$

As these losses are responsible for the decrease of energy in the system, they reduce the energy flux through the upper surface of a volume element in the system consisting of a disk of radius R and thickness δz relative to that through the lower surface, by an amount δJ where

$$\delta J\pi R^2 = -\gamma_{gg}\pi R^2\delta z - \gamma_{gw}2\pi R\delta z. \tag{2.24}$$

The resulting differential equation for the vertical component of flux, J is therefore

$$\frac{\mathrm{d}J}{\mathrm{d}z} = -\gamma_{gg} - \gamma_{gw}\frac{2}{R}. \tag{2.25}$$

With the Brey energy flux expression this can be written in dimensionless form as

$$\frac{\mathrm{d}}{\mathrm{d}z^*}\left(\kappa^*T^{*1/2}\frac{\mathrm{d}T^*}{\mathrm{d}z^*} + \mu^*\frac{T^{*3/2}}{\eta}\frac{\mathrm{d}\eta}{\mathrm{d}z^*}\right) = \frac{192\eta T^{*3/2}}{75\pi}\left(24\eta g_0(\eta)(1-e^2) + \frac{\chi(\eta)\left(1-e_w^2\right)}{\sqrt{2}R^*}\right), \tag{2.26}$$

where $R^* = R/d$.

Expanding the left-hand side of (2.26) gives

$$\kappa^*\left(\frac{\mathrm{d}^2T^*}{\mathrm{d}z^{*2}} + \frac{1}{2T^*}\left(\frac{\mathrm{d}T^*}{\mathrm{d}z^*}\right)^2\right) + \mu^*\left(\frac{T^*}{\eta}\frac{\mathrm{d}^2\eta}{\mathrm{d}z^{*2}} - \frac{T^*}{\eta^2}\left(\frac{\mathrm{d}\eta}{\mathrm{d}z^*}\right)^2 + \frac{3}{2\eta}\frac{\mathrm{d}\eta}{\mathrm{d}z^*}\frac{\mathrm{d}T^*}{\mathrm{d}z^*}\right)$$
$$= \frac{192\eta T^*}{75\pi}\left(24\eta g_0(\eta)(1-e^2) + \frac{\chi(\eta)\left(1-e_w^2\right)}{\sqrt{2}R^*}\right). \tag{2.27}$$

The final step involves expressing the second derivative of the temperature in terms of only η, T^*, $\mathrm{d}\eta/\mathrm{d}z^*$ and $\mathrm{d}T^*/\mathrm{d}z^*$; this requires substitution of (2.5), and gives (2.28):

$$\left(\mu^*\frac{(1-\eta)(1+\eta+\eta^2-\eta^3)}{(1+4\eta+4\eta^2-4\eta^3+\eta^4)} - \kappa^*\right)\frac{\mathrm{d}^2T^*}{\mathrm{d}z^{*2}}$$
$$= -\frac{192\eta T^*}{75\pi}\left(24\eta g_0(\eta)(1-e^2) + \frac{\chi(\eta)\left(1-e_w^2\right)}{\sqrt{2}R^*}\right) + \kappa^*\frac{1}{2T^*}\left(\frac{\mathrm{d}T^*}{\mathrm{d}\,z^*}\right)^2$$
$$-\mu^*\frac{T^*}{\eta^2}\left(\frac{\mathrm{d}\eta}{\mathrm{d}z^*}\right)^2 + \mu^*\frac{3}{2\eta}\frac{\mathrm{d}\eta}{\mathrm{d}z^*}\frac{\mathrm{d}T^*}{\mathrm{d}z^*} - \mu^*\frac{T^*}{\eta}f(\eta, T^*). \tag{2.28}$$

Equivalent equations to (2.26) and (2.28) for the Jenkins heat conduction model can be derived as follows:

$$\frac{\mathrm{d}}{\mathrm{d}z^*}\left(\eta T^{*1/2}\left[\frac{5}{24}\frac{1}{G}+1+\frac{6}{5}\left(1+\frac{32}{9\pi}\right)G\right]\frac{\mathrm{d}T^*}{\mathrm{d}z^*}\right) = \frac{8}{15}\frac{\eta T^{*3/2}}{\pi}\left(24\eta g_0(\eta)(1-e^2)+\frac{\chi(\eta)\left(1-e_w^2\right)}{\sqrt{2}R^*}\right) \quad (2.29)$$

$$\left[\frac{5}{24}\frac{1}{G}+1+\frac{6}{5}\left(1+\frac{32}{9\pi}\right)G\right]\frac{\mathrm{d}^2T^*}{\mathrm{d}z^{*2}} = \frac{8}{15}\frac{T^*}{\pi}\left(24\eta g_0(\eta)(1-e^2)+\frac{\chi(\eta)\left(1-e_w^2\right)}{\sqrt{2}R^*}\right) - \frac{1}{\eta}\left[\frac{5}{24}\frac{1}{G}+1+\frac{6}{5}\left(1+\frac{32}{9\pi}\right)G\right]\frac{\mathrm{d}T^*}{\mathrm{d}z^*}\frac{\mathrm{d}\eta}{\mathrm{d}z^*} - \frac{1}{2T^*}\left[\frac{5}{24}\frac{1}{G}+1+\frac{6}{5}\left(1+\frac{32}{9\pi}\right)G\right] \times\left(\frac{\mathrm{d}T^*}{\mathrm{d}z^*}\right)^2 - \left[-\frac{5}{24}\frac{1}{G^2}+\frac{6}{5}\left(1+\frac{32}{9\pi}\right)\right]\frac{\mathrm{d}T^*}{\mathrm{d}z^*}\frac{\mathrm{d}G}{\mathrm{d}z^*}. \quad (2.30)$$

Thus the system may be described in terms of T^* and η through the coupled first-order ODE (2.4) and the second-order ODE (2.28) or (2.30). These can be rewritten as three first-order ODEs in the variables η, T^* and $\mathrm{d}T^*/\mathrm{d}z^*$, from which the required profiles $\eta(z^*)$ and $T^*(z^*)$ can be calculated using standard ODE solvers. Before this can be done, however, it is necessary to specify the boundary conditions consisting of the values of η, T^* and $\mathrm{d}T^*/\mathrm{d}z^*$ at $z^*=0$. We consider how to specify these conditions in the next section.

3. Boundary conditions

Of the three required boundary conditions, only the temperature gradient can be specified directly, and this requires a suitable model relating the base excitation parameter to the energy flux at $z^*=0$, which we develop below. Neither $\eta(0)$ nor $T^*(0)$ are known *a priori*. However, two alternative conditions can be specified: first, in the limit $z^*\to\infty$, $J(z^*)\to 0$ as particles, the carriers of energy, become increasingly rare; and secondly, the total number of particles, which is proportional to $\int\eta(z^*)\,\mathrm{d}z^*$, is fixed.

We consider first the energy flux across the base of the bed, which can be used to calculate the temperature gradient at the point $z^*=0$, given boundary values for the packing fraction and temperature. At least three analyses for energy transfer rates from a moving boundary to a granular system have been proposed (Richman 1993; Warr & Huntley 1995; Kumaran 1998*b*). Warr & Huntley (1995) developed a detailed analysis to calculate the mean amount of energy transferred to a particle impacting a base vibrating with a triangular waveform, of velocity $\pm V$. This mean is obtained over all possible impact speeds (assuming a Maxwell–Boltzmann distribution), and all possible impact positions in the base cycle via an integral, I_e, which gives the mean change in velocity squared of the particles on collision and is evaluated numerically for a given base velocity magnitude. The only requirement on the vibration period is that it should be much shorter than the mean time between successive collisions made by a given particle and the base, so that the point in the base cycle at which the particle impacts is essentially random. The flux at $z^*=0$ can be specified in terms of I_e as

$$J_0=\frac{3m\eta_0\chi(\eta_0)}{(2\pi)^{3/2}d^3}\left(\frac{m}{k_BT_0}\right)^{1/2}I_e, \quad (3.1)$$

where $T_0=T(0)$ and $\eta_0=\eta(0)$.

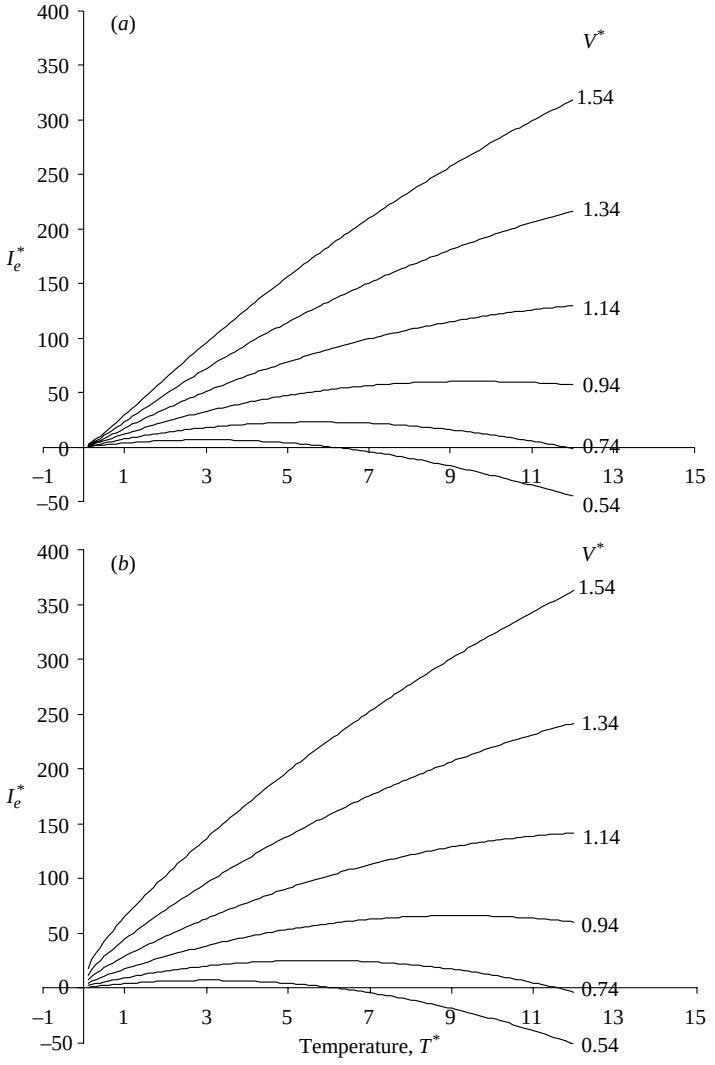

FIGURE 1. Energy input integral (I_e) for a range of base and particle impact velocities, and a base–particle restitution coefficient of 0.91 (glass base and glass particles). (*a*) Warr & Huntley model, (*b*) Richman model.

Figure 1(*a*) shows how the non-dimensional integral $I_e^* = I_e/g^2d^2$ varies depending upon the speed (temperature) of the incident particles and the dimensionless velocity of the base, $V^* = V/\sqrt{dg}$, for the case $e_w = 0.91$. It can be seen that with small base velocities, higher incident speeds do not necessarily lead to greater energy inputs, and it is possible for incident particles to lose energy on the average during an impact.

An alternative expression proposed by Kumaran (1998*b*) gives an energy input proportional to $T^{1/2}\langle V^2\rangle$, which is easy to implement, but does not allow for the possibility of energy extraction from the bed, nor does it take into account the coefficient of restitution between the particle and the base. Richman (1993) provided expressions for the mean energy input to, and that extracted from, a bed by a frictionless bumpy boundary moving in all three orthogonal directions with a mean square velocity of $3V^2$ (i.e. V^2 for each axis). The difference between these expressions

can then be used to calculate the flux for the current problem by setting the bumpiness parameter, θ, to zero. Motion of a flat frictionless base in the two in-plane (x and y) directions causes no additional transfer of energy to the granular material, and Richman's analysis (for the case of a mean square velocity of $3V^2$) should therefore be directly comparable to the Warr & Huntley analysis for a base moving in the z-direction with a velocity $\pm V$. The equivalent functional form of I_e^* is plotted in figure 1(b) for the same base velocities as in figure 1(a). Despite some differences at the low T^* end, the two sets of curves (figures 1(a) and 1(b)) are seen to be broadly equivalent. The decision on which of the two should be chosen is therefore unlikely to influence the outcome of the calculations significantly. The advantage of the Warr–Huntley expression is that, provided the assumptions noted above are satisfied, it is an exact result, taking account, for example, of double-bounce interactions with the base. On the other hand, it is only exact for a triangular waveform. For the results presented in this paper we used the Warr & Huntley flux expression, and took account of the fact that the experimental waveform is actually sinusoidal by equating the mean square velocities for the two cases (V^2 and $A_0^2\omega^2/2$, respectively).

The energy flux at the base, $J = J_0$, then leads to the following condition at $z^* = 0$, for the case of a base with the same restitution coefficient as for the particle–particle collisions:

$$J_0 = -\frac{75k_B}{64\sqrt{\pi}d^2}\left(\frac{k_BT_0}{m}\right)^{1/2}\left(\kappa^*\left.\frac{\mathrm{d}T}{\mathrm{d}z}\right|_{z=0} + \mu^*\frac{T_0}{\eta_0}\left.\frac{\mathrm{d}\eta}{\mathrm{d}z}\right|_{z=0}\right) = \frac{3m\eta_0\chi(\eta_0)}{(2\pi)^{3/2}d^3}\left(\frac{m}{k_BT_0}\right)^{1/2} I_e. \tag{3.2}$$

Substituting in (2.4) and expressing in dimensionless form results in the temperature gradient at $z^* = 0$, which is the first of the required boundary conditions:

$$\left(\mu^*\frac{(1-\eta_0)(1+\eta_0+\eta_0^2-\eta_0^3)}{(1+4\eta_0+4\eta_0^2-4\eta_0^3+\eta_0^4)} - \kappa^*\right)\left.\frac{\mathrm{d}T^*}{\mathrm{d}z^*}\right|_{z^*=0} = \frac{96\eta_0\chi(\eta_0)I_e^*}{75\sqrt{2}\pi T_0^*} - \mu^*\frac{(1-\eta_0)^4}{(1+4\eta_0+4\eta_0^2-4\eta_0^3+\eta_0^4)}. \tag{3.3}$$

The equivalent boundary condition for the Jenkins heat flux equation is

$$\left[\frac{5}{24}\frac{1}{G} + 1 + \frac{6}{5}\left(1+\frac{32}{9\pi}\right)G\right]\left.\frac{\mathrm{d}T^*}{\mathrm{d}z^*}\right|_{z^*=0} = \frac{4\chi(\eta_0)I_e^*}{15\sqrt{2}\pi T_0^*}. \tag{3.4}$$

To impose the second boundary condition, $J(\infty) = 0$, we set (2.7) (Jenkins model) or (2.9) (Brey model) to zero. This fixes the temperature gradient at the top of the system as zero in the former case, and

$$\left.\frac{\mathrm{d}T^*}{\mathrm{d}z^*}\right|_{z^*=\infty} = -\frac{\mu^*(1-\eta)^4}{(\mu^*(1-\eta)(1+\eta+\eta^2-\eta^3) - \kappa^*(1+4\eta+4\eta^2-4\eta^3+\eta^4))} \tag{3.5}$$

in the latter case. It is worth pointing out that this gradient is non-zero, and actually positive for the values of restitution coefficient used in our experiment, leading to an increasing temperature at large values of z. This results directly from the form of (2.9), and is not a consequence of the method used to solve the ODEs.

To apply both the second and third boundary conditions, it is necessary to use initial estimates for η_0 and T_0^*. The three first-order ODEs are solved, in this case using a medium-order Runge–Kutta technique (MATLAB function ode45). In general, the calculated temperature gradient at large z^* will diverge markedly from the required

value (either zero or that given by (3.5)). The initial estimate for T_0^* is then updated within an iterative scheme until the required value is satisfied at the end of the integration range ($z^* = 50$). The resulting $T^*(z^*)$ and $\eta(z^*)$ profiles then represent the solution for the case where the number of grains in the bed is

$$N = 6R^{*2} \int_0^\infty \eta\left(z^*\right) \mathrm{d}z^*. \tag{3.6}$$

In general, this will not correspond to the actual number of particles. The third boundary condition is therefore imposed by updating the initial estimate for η_0 in a second iterative loop so as to minimize the difference between the calculated N and the actual N. For each updated estimate for η_0 it is, of course, necessary to re-impose the second boundary condition above.

This method provides temperature and packing fraction distributions for given values of the number of particles, vibration amplitude, coefficients of restitution with particles, base and wall, and the size of the system. The following sections describe the comparison between such predicted distributions and those measured experimentally, together with the study of several scaling laws.

4. Comparison with experiment

The system outlined above has also been investigated experimentally in three-dimensional beds using the technique of PEPT. Seven hundred glass beads, each with a diameter of 5 mm, were placed in a 140 mm diameter polymethyl methacrylate (PMMA) container, of height 300 mm, which was fitted with a glass base. The coefficients of restitution were measured as 0.91 ± 0.02 for a glass–glass collision and 0.68 ± 0.04 for a glass–PMMA collision. The cylinder was then attached to a Ling Dynamic Systems vibrator, which vibrated the system at a frequency of 50 Hz and amplitude of up to 1.54 mm with a sinusoidal waveform. Horizontal displacements were found to be less than 3 % of the magnitude of the main vertical displacements.

PEPT involves labelling a single tracer particle with radioactive nuclei. These nuclei decay by positron emission, and the positrons emitted rapidly annihilate with local electrons, producing pairs of gamma rays travelling in opposite directions. Two position sensitive detectors placed either side of the system detect the gamma rays. A line can later be drawn between the two positions, along which the emitting particle must have lain. In theory, it takes only a single additional line to pinpoint the location of the particle, but in practice a number of events are used to correct for scattering within the system. In the system outlined above, PEPT can typically locate the tracer particle up to 500 times per second, with an accuracy of 1–2 mm when the particle is travelling at $1\,\mathrm{m\,s^{-1}}$. As the tracer particle used here was identical to all the others, apart from its radioactivity, the trajectory obtained is representative of all the particles, and can be used to calculate the system distributions. Packing fraction and temperature profiles for such a system have been published previously (Wildman *et al.* 2001) and as these publications contain details of how the profiles were obtained, they are not reproduced here.

Comparisons between the model predictions and the experimental values are plotted in figures 2 and 3. The model results in figure 2 were obtained using the Brey heat flux equation (2.9)–(2.11), whereas those in figure 3 were based on the Jenkins equation (2.7) and (2.18). The z-component of measured temperature is plotted here since this is the relevant component for this one-dimensional model. The simple heat flux

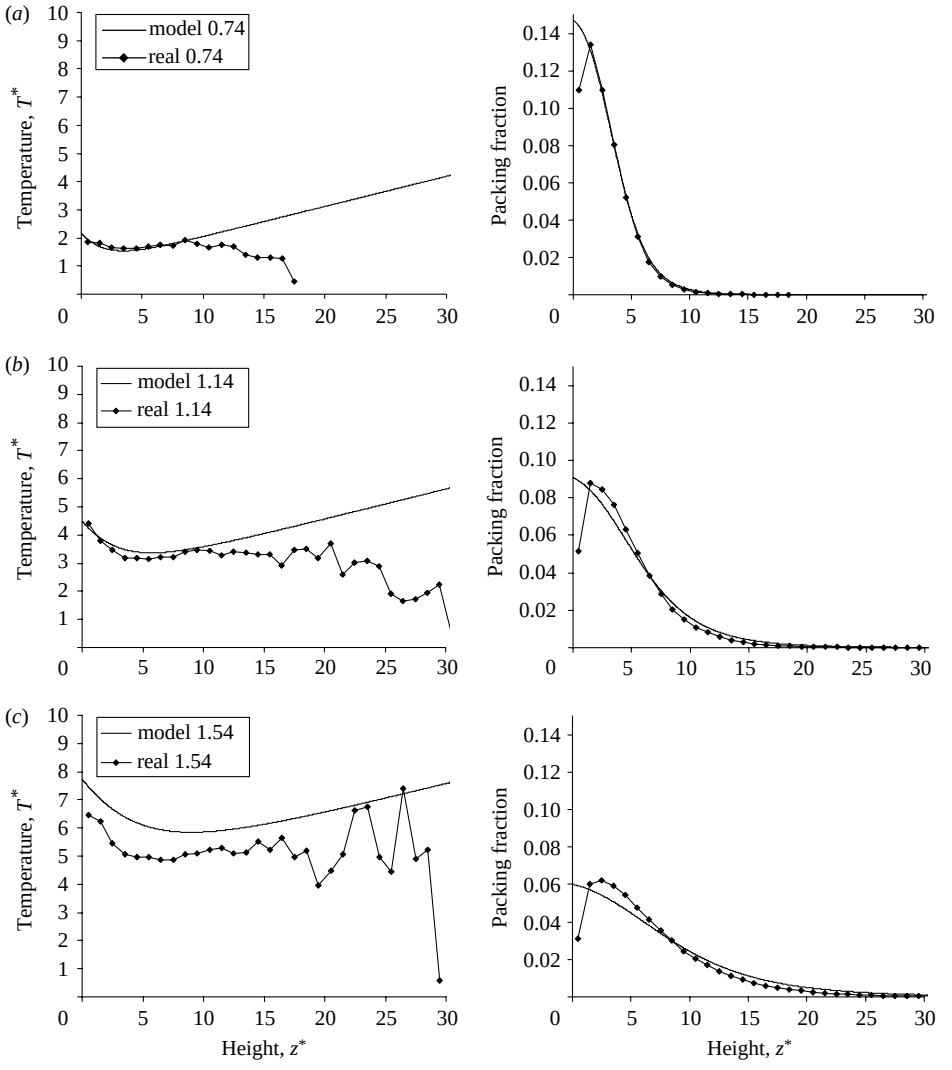

FIGURE 2. Comparisons between the model (using Brey heat flux equation) and experimental results for dimensionless temperature and packing fractions at dimensionless base velocities of (*a*) 0.74, (*b*) 1.14 and (*c*) 1.54.

equation (2.7) predicted distributions that differed significantly from the experimental ones, having a higher base temperature, and tending to a constant temperature at high levels which is much lower than that observed. The packing fraction profiles also indicated a large concentration of particles approximately four particle diameters above the base, much higher than that observed experimentally. In view of the poor agreement we have not presented the results here.

The temperatures at low $z*$ (< 3) are seen to agree slightly better when calculated with the Brey equation than with the Jenkins equation, as the temperature gradient is slightly higher, indicating that the base boundary condition (equations (3.3) and (3.4)) is better satisfied using the Brey expression; although, as the amplitude of the vibration increases, the temperatures predicted by both models increase more rapidly than those observed experimentally.

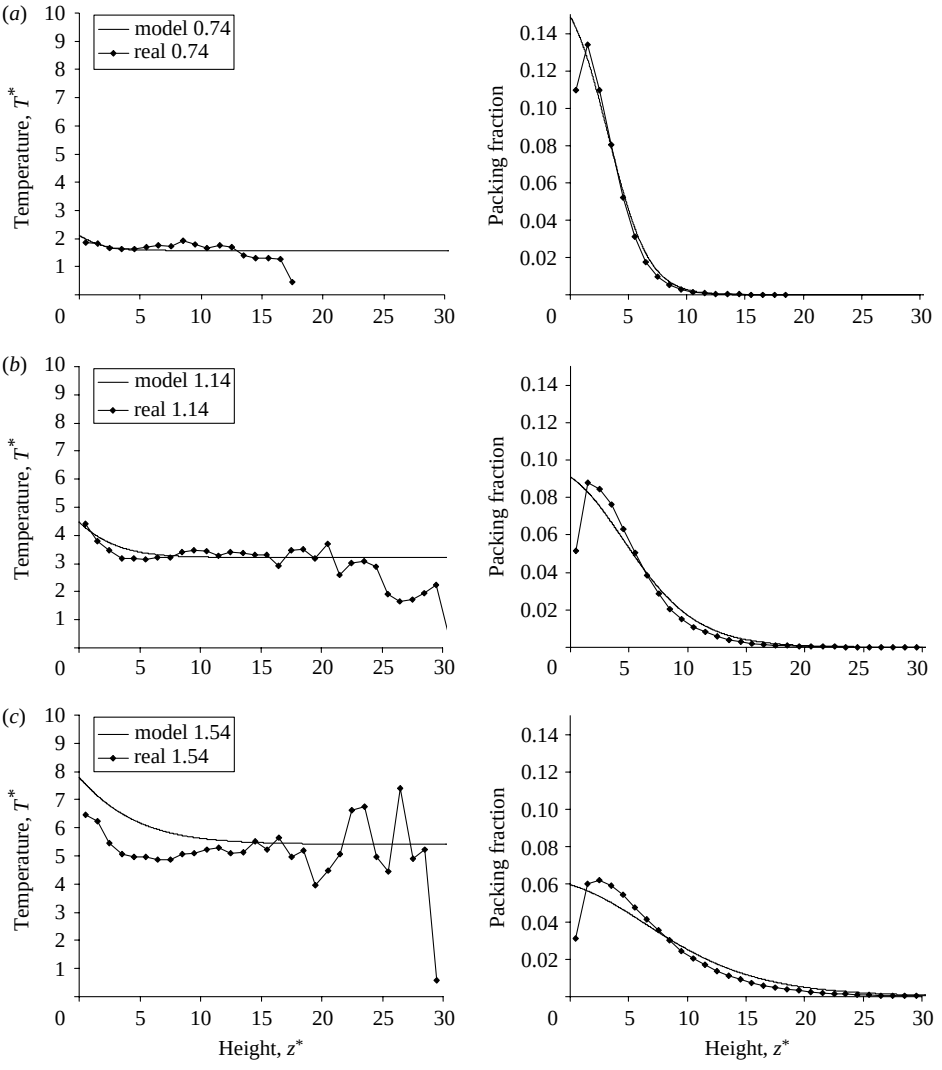

FIGURE 3. Comparisons between the model (using Jenkins heat flux equation) and experimental results for dimensionless temperature and packing fractions at dimensionless base velocities of (*a*) 0.74, (*b*) 1.14 and (*c*) 1.54.

The situation is reversed at higher $z*$ values since the experimental results show no real evidence of the upturn in temperature predicted by the Brey equation (figure 2), owing to the zero flux condition at the top of the system. However, as fewer data are gathered for the more dilute higher regions, it becomes difficult to obtain accurate temperature values in these regions. It is worth noting that slight rises in temperature have been observed previously, such as those reported by Wildman *et al.* (2001), and that there does seem to be a small dip in the 5 to 10 particle region.

The models predict, in both cases, higher packing fractions at the base than are observed experimentally. The experimental profiles demonstrate sharp dips at the base, probably due to the manner in which the PEPT algorithm locates particles next to a surface. If we neglect this artefact, the predictions from the Brey equation (figure 2) are seen to be in slightly better agreement than those of the Jenkins model, giving

N	V^*	Experimental z_m^*	Model z_m^*	Experimental T_m^*	Model T_m^*
700	0.740	3.03	2.69	1.73	1.72
700	1.142	4.94	4.76	3.45	3.71
700	1.544	7.16	7.45	5.23	6.41

TABLE 1. Comparison between observed mean bed properties and those predicted by the model.

slightly higher concentrations near the base and lower concentrations near the top, bringing them closer to the experimental results.

Two numbers are often used to describe the state of a vibrofluidized bed: the height of the centre of mass (z_m^*) and the mean temperature of the bed (T_m^*), and these collapse the distributions down to single figures. As the system is driven harder, both values increase. Table 1 shows a comparison between the values obtained from experimental data and those obtained from the model. In this case, the results from the Brey equation are used, with the granular temperature distribution weighted by the packing fraction distribution so that the high temperatures observed in the presence of few particles do not dominate the calculation. Good agreement between the two is obtained for the height of the centre of mass, while temperature behaviour is similar to the temperature trend at the base of the bed noted above.

5. Discussion

It can be seen from figures 2 and 3 and table 1 that there is reasonable agreement between the experimental results and the model, using only the measurable system properties and no adjustable parameters. There are, however, two areas where the model and the results differ significantly: first, the bulk temperature values predicted by the model increase more rapidly with increasing amplitude than do the experimental ones, and secondly, the experimental results show no rise in temperature at large z values, unlike the predictions of the Brey equation (figure 2).

There are alternative expressions for the energy input and dissipation rates, for example, Kumaran (1998*b*) energy input and Chapman & Cowling (1970) dissipation rates, although they generally have the same packing fraction and temperature dependencies, only varying slightly in the constants. However, these alternatives were not found to provide any better agreement. Higher dissipation rates, for example, give lower temperatures, and consequently better agreement with the observed temperatures for large vibration rates, but worse agreement for low rates.

Changing the equation of state used, however, changes the relationship between the two. The Carnahan & Starling (1969) equation of state shows a complex packing fraction dependence, which is why the packing fractions can agree reasonably well over a range of conditions while the temperatures systematically worsen with increasing vibration amplitude. The Carnahan & Starling (1969) equation gives better agreement than the ideal gas equation, which is why it was used here, however, there may well be alternative equations that model the system more accurately and give even better results.

The second main discrepancy is the upturn in the temperature profiles predicted by the model when using the Brey heat flux equation. This phenomenon has been observed and commented on previously by Brey, Ruiz-Montero & Moreno (2001), Ramirez & Soto (2002), and in detail in Brey & Ruiz-Montero (2004), and is the

result of (2.9), where the temperature and packing fraction gradients can balance each other to give zero flux. As commented in § 3, the scarcity of particles in this region increases the random errors in the measured temperature values, although any systematic errors are reduced as the mean free time becomes much greater than the temporal resolution of the PEPT system. A more plausible explanation for the discrepancy is that in this dilute region, it becomes highly questionable as to whether a hydrodynamic description provides a valid model for the system.

We can draw an analogy between the current situation and the case of Knudsen flow within a pipe, which occurs when the mean free path is comparable to the pipe diameter. Two possible critical packing fractions can be proposed to predict the limit of hydrodynamic applicability: the first, η_v, occurs when the mean time between collisions is large enough for gravity to completely arrest the mean particle vertical motion; and the second, η_r, occurs when the mean time between collisions exceeds the mean time required to cross a horizontal distance equal to the radius of the vessel. These relationships are;

$$\eta_v = \frac{\sqrt{\pi}}{24T^*}, \tag{5.1}$$

$$\eta_r = \frac{\sqrt{\pi}}{24}\frac{d}{R}. \tag{5.2}$$

Vertically, a situation is reached where particles are more likely to follow parabolic trajectories than to collide with each other. Given elastic particles and the assumption that particles passing this point have a range of speeds given by a Maxwell–Boltmann distribution, we would expect an isothermal region above with an exponentially decreasing packing fraction, as the particle kinetic energy is converted into potential energy; the fewer high-speed particles reach further, but their speed is reduced as they lose kinetic energy. Horizontally, the limit shows no temperature dependence, as particles that move faster collide more often, but will also cross the specified distance in a smaller time.

If we model the system crudely as consisting of a hydrodynamic regime below the relevant critical packing fraction, and collisionless parabolic trajectories above, then the variation of temperature with height in the upper region, where the assumptions giving rise to the Maxwellian velocity distribution no longer apply, can be derived as follows. Clearly, gravity will have no effect on the velocity distributions in either the x^* or y^* directions. However, in the vertical direction, gravity will prevent some of the lowest-speed particles reaching a given height z^* lying above the critical height z_c^*, and reduce the velocity of those particles that are sufficiently energetic to reach height z^*. If we consider the probability density functions $f_1(v_1)$ and $f_2(v_2)$ for the z-component of velocity, at two heights z_1 and z_2, then the dynamic interchange of particles between the two heights means that at steady state

$$n_2 f_2(v_2) = n_1 \frac{v_1}{v_2} f_1(v_1)\frac{\mathrm{d}v_1}{\mathrm{d}v_2}, \tag{5.3}$$

where n_1 and n_2 are the number per unit length at the two heights, and

$$v_2^2 = v_1^2 - 2gh \ (v_2 \geqslant 0). \tag{5.4}$$

If the velocity density at z_1 is Maxwellian, i.e.

$$f_1(v_1) = A\exp\left(-\frac{mv_1^2}{2k_BT}\right) \ (-\infty < v_1 < \infty), \tag{5.5}$$

with A the normalization constant $m/(2\pi k_B T)^{1/2}$, then from (5.3) to (5.5) it is easy to show that the corresponding function at height z_2 is

$$\left.\begin{aligned} n_2 f_2(v_2) &= n_1 \exp\left(-\frac{mg(z_2 - z_1)}{k_B T}\right) A \exp\left(-\frac{m v_2^2}{2k_B T}\right) (v_2 \geqslant 0), \\ f_2(v_2) &= f_2(-v_2)\ (v_2 < 0). \end{aligned}\right\} \tag{5.6}$$

Therefore, even though no grain–grain collisions occur between the two heights, the density function is seen to remain Maxwellian with the same temperature, and with a Boltzmann exponential decay in packing fraction. Although this analysis ignores the losses from grain–wall collisions, such losses can be shown to be relatively small. As a first-order approximation, we therefore assign constant temperature and exponential decay in packing fraction above z_c^*. This allows the total rate of energy loss due to grain–wall collisions to be calculated analytically, which can then be used as the boundary condition for energy flux at height $z^* = z_c^*$.

The result of including the above into the Brey version of the model for a base velocity V^* of 1.14 is given in figure 4. Below the limiting point, the curves are almost identical, indicating that the upper region has very little influence on the lower region. Above the limiting points, the packing fraction profiles are seen to agree much more closely with experimental results than the pure hydrodynamic prediction, which is clearly not Boltzmann-like. The constant temperature for $z^* > z_c^*$ is also much closer to the profile observed experimentally. The fact that the predictions are still slightly higher than the experimental curves suggests that the hydrodynamic approach may lose its validity at an even lower height than the limiting packing fractions used here. This approach leads to sharp changes in the gradients of the curves. In reality, of course, the transition would be smoother, as the fraction of particles undergoing insufficient collisions to be modelled by the hydrodynamic description gradually increased. The development of a suitable theory to describe the transition in a rigorous way is, however, beyond the scope of the current paper.

6. Scaling behaviour

Even with the limitations outlined above, the simple unmodified model gives good values for the height of the centre of mass (z_m^*) and mean weighted temperature (T_m^*) because the unphysical increase in temperature at high altitude is weighted by a rapidly decreasing packing fraction. The model can therefore be used to investigate the scaling behaviour of z_m^* and T_m^* with the base velocity, number of particles and particle–particle restitution coefficient. Figure 5 illustrates how these values vary for a range of base velocities and number of particles within the system. Both of these values increase with increasing excitation and decrease with increasing numbers of particles. The reason for this is in the energy balance; higher base velocities lead to a greater energy input into the system, giving higher temperatures and more dilated beds, while systems with more particles have more collisions and their energy is dissipated more quickly, leading to lower mean values.

Figures 6 and 7 show how the height of the centre of mass and mean weighted temperature, respectively, change when the hydrodynamic limits are imposed. The radial limit changes these properties only slightly (less than 3 %), and has most impact on beds with fewer particles, where the systems naturally have a lower packing fraction distribution so the limit is reached at a lower height, changing more of the distribution. The vertical limit is temperature dependent and so the beds with low excitation levels reach their limiting heights sooner, along with those beds with

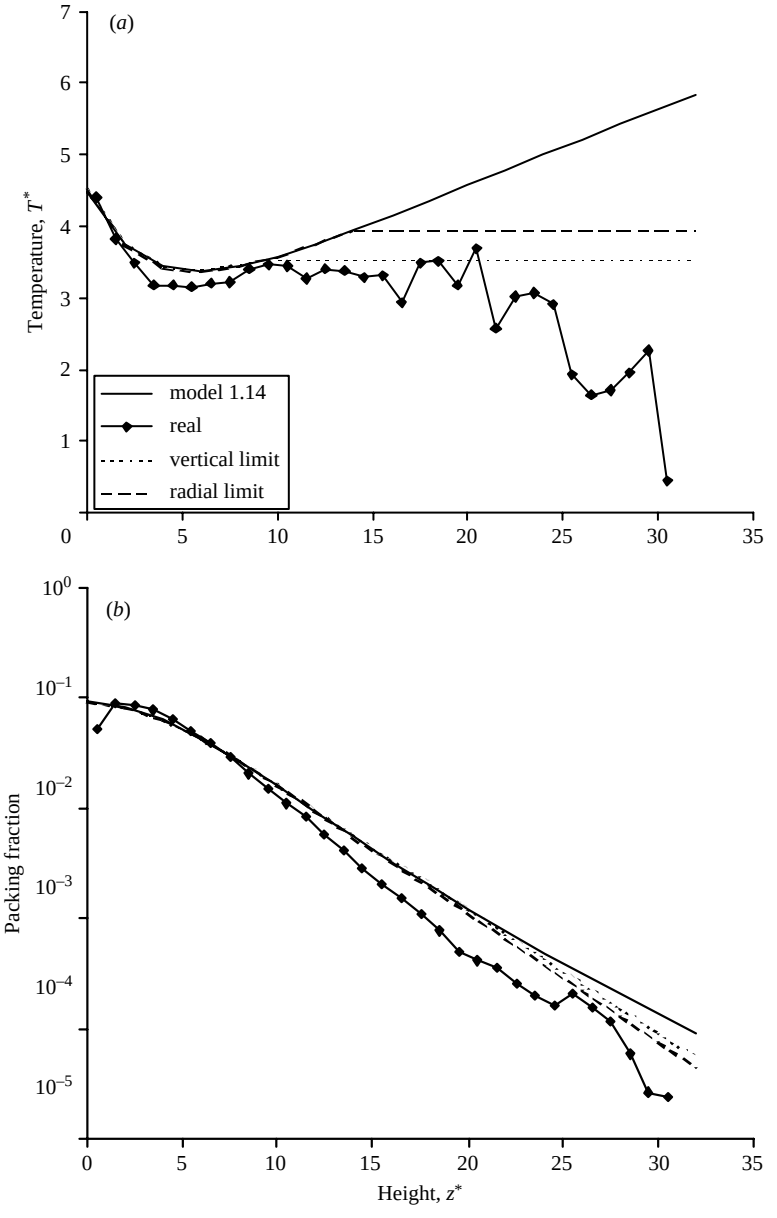

FIGURE 4. (*a*) dimensionless temperature and (*b*) packing fraction profiles using the two definitions for the transition point to the Knudsen regime.

fewer particles, so these show the most change; as much as 8 % difference for a bed with 350 particles at a base velocity of 0.74. However, since the changes are small, it would seem reasonable to use the simple model to obtain an idea of bed behaviour under varying conditions.

In many cases (Warr & Huntley 1995; Kumaran 1998*b*), the dissipation due to wall impacts is not included in models to estimate these two values. In this model, it is simple to turn the wall dissipation off by setting the wall coefficient of restitution to 1, and an illustration of how these values change in this situation, using this simple

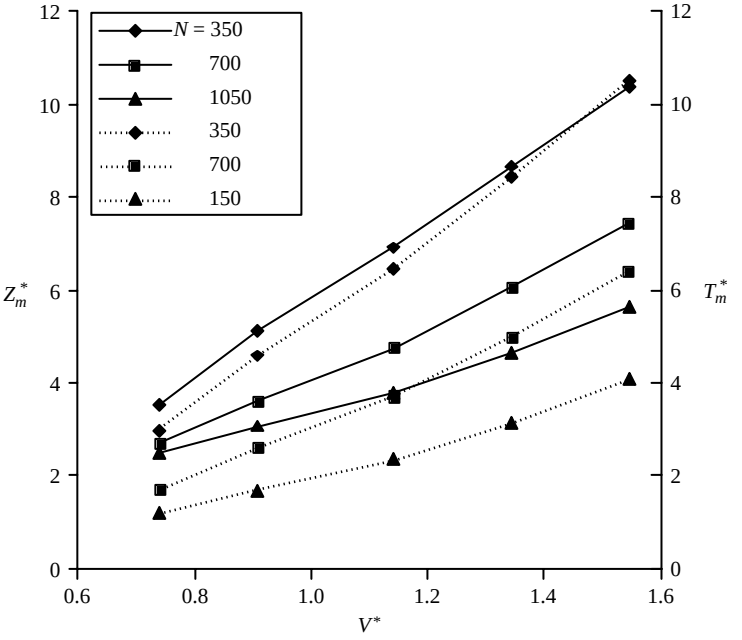

FIGURE 5. Height of centre of mass (Z_m^*, solid line) and weighted mean bed temperature (T_m^*, dashed line) predicted by the model for various base velocities.

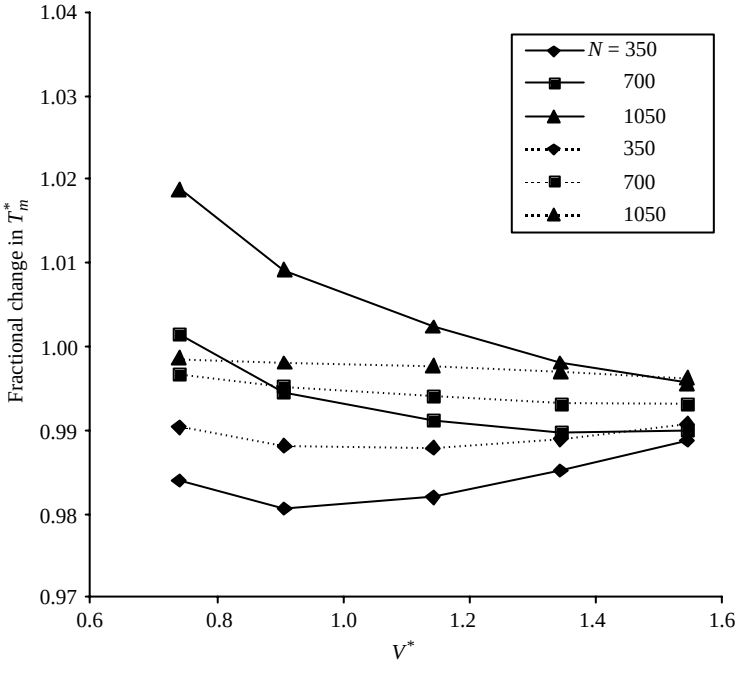

FIGURE 6. Fractional change in weighted mean bed temperature for models using vertical (solid lines) and radial (dashed lines) limits for the hydrodynamic description of bed behaviour compared to the basic model.

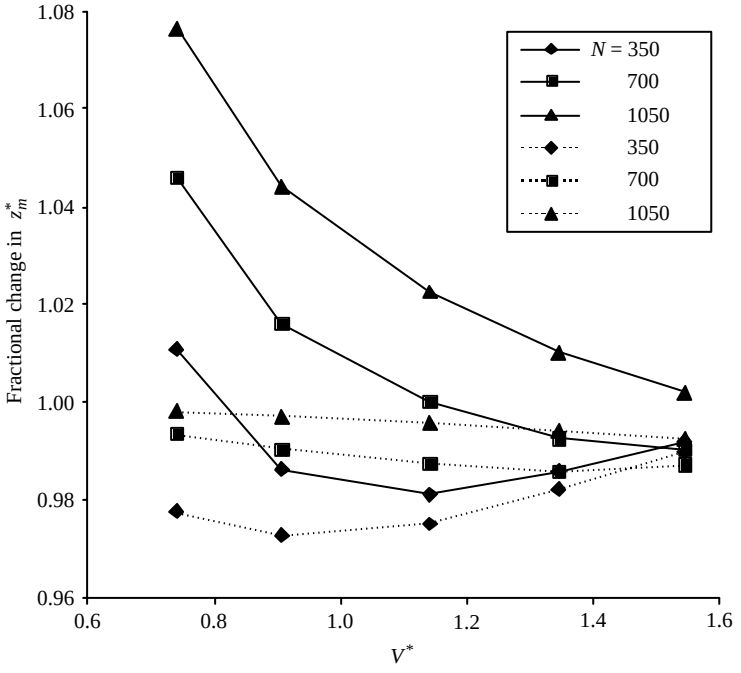

FIGURE 7. Fractional change in height of centre of mass for models using vertical (solid lines) and radial (dashed lines) limits for the hydrodynamic description of bed behaviour compared to the basic model.

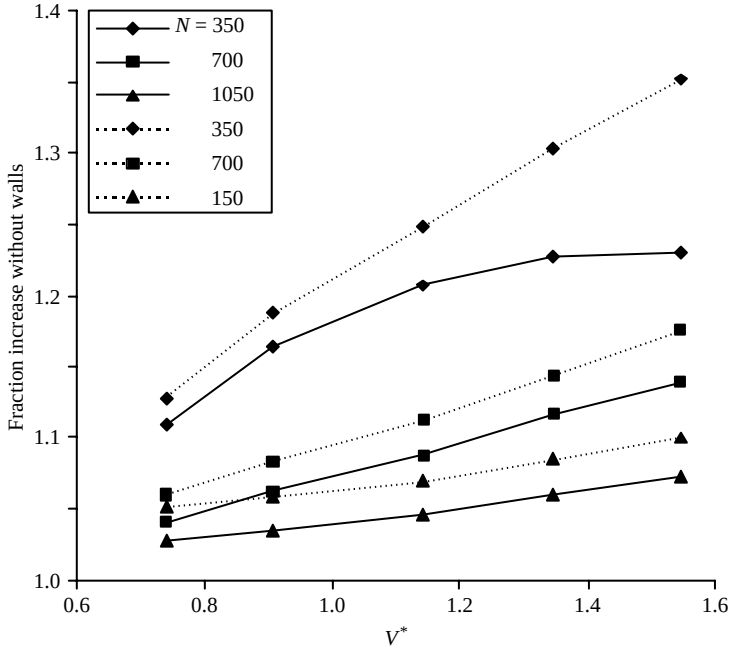

FIGURE 8. Increase in weighted mean bed temperature (T_m^*, dashed line) and height of centre of mass (Z_m^*, solid line) predicted by the model for a system with no wall dissipation.

Property		Wall dissipation	Dimensions	N exponent	V^* exponent
z_m^*	Current model	Y	3	-0.47 ± 0.14	1.29 ± 0.20
z_m^*	Wildman *et al.* (2001) experiment	Y	3	-0.37 ± 0.09	1.24 ± 0.15
z_m^*	Warr *et al.* (1995) experiment	Y	2	-0.27 ± 0.11	1.3 ± 0.04
z_m^*	Current model	N	3	-0.58 ± 0.17	1.40 ± 0.24
z_m^*	Warr *et al.* (1995) model	N	2	-1	2
z_m^*	Luding *et al.* (1994*b*) simulation	N	2	-1	1.5
T_m^*	Current model	Y	3	-0.87 ± 0.04	1.69 ± 0.06
T_m^*	Wildman *et al.* (2001) experiment	Y	3	-0.76 ± 0.07	1.54 ± 0.37
T_m^*	Warr *et al.* (1995) experiment	Y	2	-0.6 ± 0.03	1.41 ± 0.03
T_m^*	Current model	N	3	-0.99 ± 0.09	1.85 ± 0.11
T_m^*	Kumaran *et al.* (1998*b*) model	N	3	-1	2
T_m^*	Warr *et al.* (1995) model	N	2	-1	2

TABLE 2. Comparison of model and experimental relationships.

model, is given in figure 8. Obviously, with less dissipation, both values increase, however, the range of increase in the systems modelled varies from 2 % to 40 %, with the more highly populated systems changing less. This demonstrates that wall impacts are a more important energy sink in dilute systems with fewer particles, where inter-particle collisions happen less frequently.

Since wall dissipation is often not included in models, but is present in experiments, values with and without it have been used to calculate the scaling dependence of the height of the centre of mass and mean weighted temperature with both the total number of particles, N, and the base velocity, V. The exponents obtained for scaling are summarised in table 2 along with values obtained by other authors. The exponents for temperature scaling agree with the models of Warr *et al.* (1995) and Kumaran (1998*b*). Most models and experiments show a centre of mass dependence of just under 1.5 on V^*, and the one presented here is no exception, and while the N exponent calculated here is in agreement with previous experimental results, previous models have predicted a factor of –1.

7. Conclusions

A one-dimensional hydrodynamic model has been developed for the prediction of granular temperature and packing fraction profiles within a three-dimensional vibrofluidized bed. Several equations from the literature for both energy input rate and for the heat flux transfer properties of the granular material have been compared. The particle–particle, particle–base, and particle–wall restitution coefficients, together with the base velocity, cell geometry, and number of particles, are included explicitly in the model allowing direct calculations to be made without any adjustable parameters.

The results were found to agree reasonably well with profiles derived experimentally using the technique of PEPT. At low excitation levels, the temperatures agree well, while packing fractions agree over the full range of excitation levels studied. It is thought that a more suitable equation of state would produce better agreement. Results from the version of the model that includes an additional term in the packing fraction gradient were found, in general, to be in slightly better agreement than those from the version without the term, although effects due to anisotropic temperature distributions, wall friction, etc. could well be sufficiently large to explain

such discrepancies. One major remaining discrepancy, however, was that the model with the extra term predicts a steadily increasing temperature at high altitudes. This unphysical behaviour can be interpreted as being due to use of the hydrodynamic approach in regions where the packing fraction is so low that the approach is no longer strictly applicable. Criteria for the onset of the Knudsen regime were proposed, and the resulting temperature profiles were found to agree more closely with the experimental distributions.

The height of the centre of mass predicted by the model agrees well with experimental results, while the predicted weighted mean temperature becomes less accurate with increasing excitation levels. The model can be used to evaluate these properties over a range of operating conditions, leading to the derivation of simple scaling laws. Compared to detailed simulations, this approach gives a quick solution for the temperature and packing fraction distributions, and it is hoped that with refinement, in particular with the inclusion of terms able to describe the transition from the hydrodynamic to the Knudsen regimes, the accuracy will improve still further.

The authors would like to acknowledge useful discussions with M. D. Shattuck, J. T. Jenkins and V. Kumaran during the Isaac Newton Institute program on Granular and Particle Laden Flows (September–December 2003, Cambridge, UK), Dr Brey for his useful comment on our implementation of his theory; the help of Dr D. J. Parker, of the Positron Imaging Centre, Birmingham University, with the PEPT experiments; and the financial support of the EPSRC through research grant GR/N34208/01. J. M. H. is also grateful to the Royal Society and Wolfson Foundation for a Royal Society–Wolfson Research Merit Award.

REFERENCES

Bizon, C., Shattuck, M. D., Swift, J. B. & Swinney, H. L. 1999 Transport coefficients for granular media from molecular dynamics simulations. *Phys. Rev.* E **60**, 4340–4351.

Brey, J. J., Dufty, J. W., Kim, C. S. & Santos, A. 1998 Hydrodynamics for a granular flow at low density. *Phys. Rev.* E **58**, 4638–4653.

Brey, J. J., Moreno F. & Dufty, J. W. 1996. Model kinetic equation for low-density granular flow. *Phys. Rev.* E **54**, 445–456.

Brey, J. J., Ruiz-Montero, M. J. & Moreno, F. 2001 Hydrodynamics of an open vibrated granular system. *Phys. Rev.* E **63**, 61305-1–61305-10.

Brey, J. J. & Ruiz-Monero, M. J. 2004 Heat flux and upper boundary condition in an open fluidized granular gas. *Europhys. Lett.* **66**, 805–811.

Carnahan, N. F. & Starling, K. E. 1969 Equation of state for nonattracting rigid spheres. *J. Chem. Phys.* **51**, 635–636.

Chapman, S. & Cowling, T. G. 1970 *The Mathematical Theory of Non-Uniform Gases*, 3rd edn. Cambridge University Press.

Clément, E., Vanel, L., Rajchenbach, J. & Duran, J. 1996 Pattern formation in a vibrated two-dimensional granular layer. *Phys. Rev.* E **53**, 2972–2975.

Helal, K., Biben, T. & Hansen, J.-P. 1997 Local fluctuations in a fluidised granular media. *Physica* A **240**, 361–373.

Horluck, S. & Dimon, P. 2001 Grain dynamics in a two-dimensional granular flow. *Phys. Rev.* E **63**, 31301-1–31301-16.

Jenkins, J. T. 1999 Kinetic theory for nearly elastic spheres. In *Physics of Dry Granular Media* (ed. H. J. Herrman, J.-P. Hovi & S. Luding), pp. 353–370. Kluwer.

Jenkins, J. T. & Savage, S. B. 1983 A theory for the rapid flow of identical, smooth, nearly elastic, spherical particles. *J. Fluid Mech.* **130**, 187–202.

Kay, J. M. & Neddermann, R. M. 1985. *Fluid Mechanics and Transfer Processes.* Cambridge University Press.

Kumaran, V. 1998*a* Kinetic theory for a vibro-fluidized bed. *J. Fluid Mech.* **364**, 163–185.

Kumaran, V. 1998*b* Temperature of a granular material 'fluidised' by external vibrations. *Phys. Rev.* E **57**, 5660–5664.

Lan, Y. & Rosato, A. D. 1995 Macroscopic behavior of vibrating beds of smooth inelastic spheres. *Phys. Fluids* **7** 1818–1831.

Luding, S., Clement, E., Blumen, A., Rajchenbach, J. & Duran, J. 1994*a* Studies of columns of beads under external vibrations. *Phys. Rev.* E **49**, 1634–1646.

Luding, S., Herrmann, H. J. & Blumen, A. 1994*b* Simulations of two-dimensional arrays of beads under external vibrations: scaling behaviour. *Phys. Rev.* E **50**, 3100–3108.

Pasquarell, G. C. & Ackermann, N. L. 1989 Boundary conditions for planar granular flows. *J. Engng Mech.* **176**, 67–94.

Ramirez, R. & Soto, R. 2002 Temperature inversion on granular fluids under gravity. *Physica* A **322**, 73–80.

Richman, M. W. 1993 Boundary-conditions for granular flows at randomly fluctuating bumpy boundaries. *Mech. Mat.* **16**, 211–218.

Warr, S. & Huntley J. M. 1995 Energy input and scaling laws for a single particle vibrating in one dimension. *Phys. Rev.* E **52**, 5596–5601.

Warr, S., Huntley, J. M. & Jacques, G. T. H. 1995 Fluidization of a two-dimensional granular system: experimental study and scaling behaviour. *Phys. Rev.* E **52**, 5583–5595.

Wildman, R. D. & Huntley, J. M. 2000 Novel method for measurement of granular temperature distributions in two-dimensional vibro-fluidised beds. *Powder Technol.* **113**, 14–22.

Wildman, R. D., Huntley, J. M., Hansen, J.-P., Parker, D. J., & Allen, D. A. 2000 Single particle motion in three dimensional vibrofluidized granular beds. *Phys. Rev.* E **62**, 3826–3835.

Wildman, R. D., Huntley, J. M., & Parker, D. J. 2001 Granular temperature profiles in three dimensional vibrofluidized beds. *Phys. Rev.* E **63**, 061311-1–061311-10.

Yang, X., Huan C., Candela, D., Mair, R. W. & Walsworth, R. L. 2002 Measurements of grain motion in a dense, three-dimensional granular fluid. *Phys. Rev. Lett.* **88**, 44301-1–44301-4.